mathematics

MDPI

Article

Mixed Isogeometric Analysis of the Brinkman Equation

Lahcen El Ouadefli [1], Omar El Moutea [2], Abdeslam El Akkad [1,3], Ahmed Elkhalfi [1], Sorin Vlase [4] and Maria Luminița Scutaru [5,*]

[1] Mechanical Engineering Laboratory, Faculty of Sciences and Techniques, B.P. 2202 Route Imouzzer, Fes 30000, Morocco; lahcen.elouadefli@usmba.ac.ma (L.E.O.); elakkadabdeslam@usmba.ac.ma (A.E.A.); ahmed.elkhalfi@usmba.ac.ma (A.E.)
[2] Laboratory of Mathematics and Applications ENS, Hassan II University Casablanca, Casablanca 20000, Morocco; moutea.omar@usmba.ac.ma
[3] Département de Mathématiques, Centre Régional des Métiers d'Education et de Formation de Fès Meknès (CRMEF Fès-Meknès), Rue de Koweit 49, Ville Nouvelle, Fez 30050, Morocco
[4] Department of Mechanical Engineering, Faculty of Mechanical Engineering, Transylvania University of Brasov, B-dul Eroilor 29, 500036 Brasov, Romania; svlase@unitbv.ro
[5] Faculty of Mechanical Engineering, Transilvania University of Brasov, 500019 Brașov, Romania
* Correspondence: lscutaru@unitbv.ro

Abstract: This study focuses on numerical solution to the Brinkman equation with mixed Dirichlet–Neumann boundary conditions utilizing isogeometric analysis (IGA) based on non-uniform rational B-splines (NURBS) within the Galerkin method framework. The authors suggest using different choices of compatible NURBS spaces, which may be considered a generalization of traditional finite element spaces for velocity and pressure approximation. In order to investigate the numerical properties of the suggested elements, two numerical experiments based on a square and a quarter of an annulus are discussed. The preliminary results for the Stokes problem are presented in References.

Keywords: Brinkman; convergence; finite element; isogeometric analysis; Nédélec; NURBS; Raviart–Thomas; Taylor–Hood

MSC: 65N30; 65N15; 65G99; 76D07; 76D99

Citation: Ouadefli, L.E.; Moutea, O.E.; Akkad, A.E.; Elkhalfi, A.; Vlase, S.; Scutaru, M.L. Mixed Isogeometric Analysis of the Brinkman Equation. *Mathematics* **2023**, *11*, 2750. https://doi.org/10.3390/math11122750

Academic Editor: Andrey Amosov

Received: 19 May 2023
Revised: 12 June 2023
Accepted: 13 June 2023
Published: 17 June 2023

1. Introduction

Hughes et al. recently developed a computational technique known as isogeometric analysis (IGA) (see [1–4]), which combines computer-aided design (CAD) and finite element analysis (FEA). The same functions that describe the computational domain in a CAD system are used in IGA to represent the solution. IGA is accurate and effective, and is a novel numerical technique used to discretize the wide range of problems of partial differential equations (PDEs). Additionally, IGA provides benefits for numerically approximating high-order PDEs using the traditional Galerkin formulation because it uses a globally smooth foundation. In particular, we refer to NURBS-based IGA because of the wide use of NURBS in CAD technology, and especially for the mathematical properties of these basic functions, for CAD models suitable for analysis. Another advantage of IGA is the use the same initial geometry throughout mesh refinement (for more details, see [4–10]).

When fissures, bulges, or channels exist in a porous matrix, the Brinkman system controls the viscous fluid in these types of inhomogeneous mediums. This system is mathematically described as a superposition of the Stokes and Darcy systems. The Brinkman problem is represented as a system of partial differential equations with a saddle point structure (for more on this type of problem, see [11–15]). As stated in [16], it is difficult to develop approximations using finite elements that behave consistently well across the spectrum of regimes (dominated by Stokes or Darcy); a collection of representative references includes [17–28].

In this study, we examine the ability of the IGA method to solve Brinkman flow problems. When discretizing the Brinkman problem, the velocity and pressure spaces must satisfy the inf-sup condition (or LBB) to ensure discretization that is free of blocking and spurious oscillations [1,2,29–31]. B-splines or NURBS on structured meshes provide flexibility in the construction of inf-sup stable- and pressure-velocity spaces with arbitrary ordering and various regularities in the context of IGA. Utilizing three significant families of isogeometric mixed elements, we examine the performance of IGA in mixed formulation elements: Taylor–Hood [1,2,32], Nédélec [1] and Raviart–Thomas [1,3]. Previous studies have explored the application of mixed isogeometric analysis in saddle point problems and fluid mechanics. The stability of the Stokes problem for these three families has been proven in [1,2,29]. Raviart–Thomas elements were used in [3] to solve the generalized Stokes problem, where stability and error estimates were established using this type of element. Additionally [33–37], investigated the use of Raviart–Thomas elements for the Navier–Stokes equations in both steady and unsteady cases, where stability and approximation estimation were established, and an a posteriori error estimate was provided.

This passage describes a research paper that presents a numerical study and comparison of different families of elements that are used to solve a Brinkman problem. The analysis of the Brinkman problem uses divergence-conforming B-splines, which can be understood as smooth generalizations of Raviart–Thomas elements, and is discussed in reference [3]. This paper extends the Galerkin Isogeometric Analysis (GIA) approach by applying smooth generalizations of Taylor–Hood and Nédélec elements in the context of NURBS functions and presenting a comparison between these compatible families. Our study provides valuable information about the capabilities of these families of elements.

This paper is organized into several sections. Section 2 provides preliminary information about splines and Non-Uniform Rational B-Splines (NURBS). Section 3 introduces mixed isogeometric spaces. Section 4 describes the discretization of the Brinkman equation using the NURBS-based finite element method. Finally, in Section 5, two numerical experiments based on a square and a quarter of an annulus are discussed.

2. NURBS and Preliminaries Results

In this section, definitions and notations related to B-splines and NURBS are presented, and more detailed descriptions can be found in [6,9,38–42] and the references therein. In the context of B-splines/NURBS, an additional domain takes into account the domain of parametric splines $\hat{\Omega}$ (see Figure 1), as opposed to finite element analysis, in which only two domains are used; the first is reference $\widetilde{\Omega}$ and the second is physical Ω. We follow this requirement and present an overview of the characteristics of spline-based discrete approximation spaces in the following.

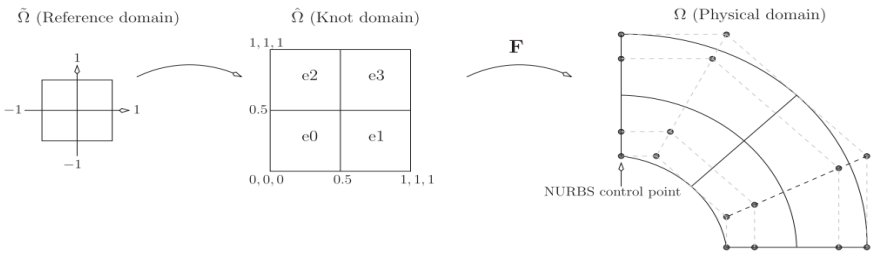

Figure 1. Domains of Isogeometric Analysis: $\widetilde{\Omega}$ is the reference domain, $\hat{\Omega}$ is the parametric domain and Ω is the physical domain defined by the parameterization **F** as an image of $\hat{\Omega}$.

B-Spline and NURBS Functions

Assuming that p and n represent two positive integers, the knots vector ε is defined as:

$$\varepsilon = \{\xi_1 = 0, \ldots, \xi_i, \ldots, \xi_{n+p+1} = 1\}, \tag{1}$$

where $(\xi_i)_i$ is the ordered sequence of the real numbers, and ξ_i is called the ith knot.

The univariate B-spline basis function $N^{p}_{\alpha,i}(\xi)$ for a given knots vector ε, can be built using the Cox–de Boor formulation (see [6]) for $p = 0$:

$$N^{0}_{\alpha,i}(\xi) = \begin{cases} 1, & \text{if } \xi_i \leqslant \xi < \xi_{i+1}, \\ 0, & \text{otherwise,} \end{cases} , \tag{2}$$

and for $p \geqslant 1$:

$$N^{p}_{\alpha,i}(\xi) = \frac{\xi - \xi_i}{\xi_{i+p} - \xi_i} N^{p-1}_{\alpha,i}(\xi) + \frac{\xi_{i+p+1} - \xi}{\xi_{i+p+1} - \xi_{i+1}} N^{p-1}_{\alpha,i+1}(\xi). \tag{3}$$

A spline curve $C(\xi)$ of order p in two dimensions is a linear combination of the control points $\mathbf{P}_i$ and the B-spline basis functions as follows:

$$C(\xi) = \sum_{i}^{n} N^{p}_{\alpha,i}(\xi)\mathbf{P}_i. \tag{4}$$

Now, let us introduce the vector of knots without repetitions $\Xi = \{\zeta_1 = 0, \ldots, \zeta_i, \ldots, \zeta_m = 1\}$ and the corresponding vector of knots multiplicities $\{r_1, \ldots, r_i, \ldots, r_m\}$. The knots vector Ξ is said to be open if $r_1 = r_m = p + 1$. At each point ζ_i, the B-spline basis functions have $\alpha_i = p - r_i$ continuous derivatives.

The univariate spline space in the $\hat{\Omega} = [0, 1]$ parametric domain, spanned by the B-splines $N^{p}_{\alpha,i}$, is denoted as:

$$\hat{\mathcal{N}}^{p}_{\alpha} := \text{span}\{N^{p}_{i}\}^{m}_{i=1}. \tag{5}$$

Let N^{p}_{i} and N^{q}_{j} be two B-splines associated with the knots vector $\varepsilon = \{\xi_1 = 0, \ldots, \xi_i, \ldots, \xi_{n+p+1} = 1\}$ and $\eta = \{\xi_1 = 0, \ldots, \xi_j, \ldots, \xi_{m+q+1} = 1\}$, respectively. The multivariate spline space in the parametric domain $\hat{\Omega} = [0, 1] \times [0, 1]$, which will be referred to as a patch, is defined using the tensor product.

$$\hat{\mathcal{N}}^{p}_{\alpha} := \text{span}\{N^{p,q}_{i,j}\}^{m,n}_{i,j=1}, \tag{6}$$

where $N^{p,q}_{i,j} = N^{p}_{i} \otimes N^{q}_{j}$, for $i = 1, \ldots, m$, $j = 1, \ldots, n$.

The 1-dimensional NURBS basis functions are introduced as:

$$R^{p}_{i}(\xi) = \frac{N^{p}_{i}(\xi)w_i}{\sum_{j=1}^{n} N^{p}_{j}(\xi)w_i}, \tag{7}$$

where w_i is the weight that was given to the ith control point, which cannot be negative. A NURBS curve $\hat{C}(\xi)$ of order p in two dimensions is a linear combination of the control points $\mathbf{P}_i$ and the NURBS basis functions, i.e.,

$$\hat{C}(\xi) = \sum_{i=1}^{n} R^{p}_{i}(\xi)\mathbf{P}_i, \tag{8}$$

The univariate NURBS space in the parametric domain $\hat{\Omega} = [0, 1]$ spanned by the NURBS basis functions R^{p}_{i} is denoted as:

$$\hat{\mathcal{N}}^{p}_{\alpha} := \text{span}\{R^{p}_{i}\}^{n}_{i=1}. \tag{9}$$

Remark 1. *The NURBS basis functions satisfy the following proprieties:*

1. *Non-negativity:* $R^{p}_{i}(\xi) \geqslant 0$.
2. *Partition of unity:* $\sum_{i=1}^{n} R^{p}_{i}(\xi) = 1$.
3. *Let* m_i *be the multiplicity of the value of* ξ_i *in the knot vector;* R^{p}_{i} *is* $\alpha_i = p - m_i$ *times continuously differentiable over a knot* ξ_i.
4. $R^{p}_{i}(\xi) = 0$, *if* $\xi \notin [\xi_i, \xi_{i+p+1}]$.

Let R_i^p and R_j^q be two NURBS basis functions associated with knot vectors $\varepsilon = \{\xi_{1,1} = 0, \ldots, \xi_{1,i}, \ldots, \xi_{1,n+p+1} = 1\}$ and $\eta = \{\xi_{2,1} = 0, \ldots, \xi_{2,j}, \ldots, \xi_{2,m+q+1} = 1\}$, respectively. The mesh Q_h associated with the knot vectors ε and η is a partition of $[0,1] \times [0,1]$ into rectangles.

$$Q_h := \{Q = (\xi_{1,i}, \xi_{1,i+1}) \otimes (\xi_{2,j}, \xi_{2,j+1}),\ i = 1, \ldots, n \text{ and } j = 1, \ldots, m\ \}, \tag{10}$$

We set the global mesh size as:

$$h := \max\{h_Q = diam(Q),\ Q \in Q_h\}, \tag{11}$$

The multivariate NURBS space in the parametric domain $\hat{\Omega} = [0,1] \times [0,1]$ is defined as:

$$\hat{\mathcal{N}}^{p,q}_{\alpha_1,\alpha_2} := \text{span}\{R^{p,q}_{i,j}\}^{n,m}_{i,j=1}, \tag{12}$$

where $R^{p,q}_{i,j} = \frac{N^p_{\alpha_1,i}(\xi) M^q_{\alpha_2,i}(\eta) w_{i,j}}{\sum_{\hat{i}}^{n} \sum_{\hat{j}}^{m} N^p_{\alpha_1,\hat{i}}(\xi) M^q_{\alpha_2,\hat{j}}(\eta) w_{i,j}}$; note that the weight $w_{i,j}$ is not defined using the tensor product.

The NURBS geometrical map $\mathbf{F} : \hat{\Omega} \to \Omega$ is then provided as follows:

$$\mathbf{F} = \sum_{i,j=1}^{n,m} R^{p,q}_{i,j}(\xi) \mathbf{P}_{i,j}, \tag{13}$$

where $\mathbf{P}_{i,j}$ refers to the control points. With the piecewise smooth inverse, the family of mesh K_h is naturally generated by $\mathbf{F}$ on the physical domain, for example,

$$K_h = \{K :\ K = \mathbf{F}(Q),\ Q \in Q_h\}, \tag{14}$$

where Q is the pre-mage of K by $\mathbf{F}$, the global mesh size is defined as follows:

$$h = max\{h_K,\ K\ \in K_h\}, \tag{15}$$

where $h_K = \| D\mathbf{F} \|_{L^\infty(Q)}\ h_K$.

The NURBS space $\mathcal{R}$ on Ω represents a push-forward of the space $\hat{\mathcal{N}}$ of NURBS on the parametric domain (patch) $\hat{\Omega}$.

$$\mathcal{R}^{p,q}_{\alpha_1,\alpha_2} := \text{span}\{R^{p,q}_{i,j} \circ \mathbf{F}^{-1} \mid i = 1, \ldots, n-1; j = 1, \ldots, m-1\}. \tag{16}$$

3. Isogeometric Spaces

It is essential that the discrete condition inf-sup be respected before putting the description of our problem into action. Here, we follow the main points of article [1], which proposed three space spline configurations that are variations of known stable spaces for traditional finite elements: Taylor–Hood likes NURBS (TH), Nédélec likes NURBS (NE) and Raviart–Thomas likes NURBS (RT). This section provides a summary of their definitions and properties; for more information, see [29].

3.1. Taylor–Hood Space

The Raviart–Thomas (RT) NURBS spaces are described as

$$\begin{cases} \hat{\mathcal{V}}^{TH}_h & := \hat{\mathcal{N}}^{p+1,p+1}_{\alpha_1,\alpha_2} \times \hat{\mathcal{N}}^{p+1,p+1}_{\alpha_1,\alpha_2}, \\ \hat{\mathcal{P}}^{TH}_h & := \hat{\mathcal{N}}^{p,p}_{\alpha_1,\alpha_2}. \end{cases} \tag{17}$$

The pressure and velocity are defined with the same regularity on the same knot mesh. The two velocity components are defined in the same space. One order lower than the velocity space is the pressure space. As a result, the velocity space has one more knot than

the pressure space; hence, we additionally need a constrained discrete velocity space to handle the no-penetration boundary condition.

$$\hat{\mathcal{V}}_{h,0}^{TH} := \{\hat{\mathbf{v}}_h \in \hat{\mathcal{V}}_h^{TH} \mid \hat{\mathbf{v}}_h = 0 \text{ on } \partial\hat{\Omega}\}, \tag{18}$$

The $\hat{\mathcal{V}}_h^{TH}$ space is spanned by:

$$\hat{\mathcal{V}}_h^{TH} := \text{span}\{\mathfrak{e}_k R_{i,j}^{\mathbf{p}+1,p+1} \mid i = 1,\dots,n; j = 1,\dots,m; k = 1,2\}, \tag{19}$$

where $\mathfrak{e}_k$ is the kth canonical basis vector of $\mathbb{R}^2$, and $\hat{\mathcal{V}}_{h,0}^{TH}$ is then spanned by:

$$\hat{\mathcal{V}}_{h,0}^{TH} := \text{span}\{\mathfrak{e}_k R_{i,j}^{p+1,p+1} \mid i = 2,\dots,n-1; j = 2,\dots,m-1; k = 1,2\}, \tag{20}$$

We assume that in $n_{V,1}^{TH} = n_{V,2}^{TH} := (n-2)(m-2)$, the space $\hat{\mathcal{V}}_{h,0}^{TH}$ is rewritten in simple notation as:

$$\hat{\mathcal{V}}_{h,0}^{TH} := \text{span}\,\{\mathfrak{e}_k R_{\mathbf{i}}^{p+1,p+1} \mid \mathbf{i} = 1,\dots,n_{V,k}^{TH}; k = 1,2\}. \tag{21}$$

The $\hat{\mathcal{P}}_h^{TH}$ space is spanned as:

$$\hat{\mathcal{P}}_h^{TH} := \text{span}\,\{R_{i,j}^{p,p} \mid i = 1,\dots,n; j = 1,\dots,m\}, \tag{22}$$

In the simple notation, we rewrite the pressure space $\hat{\mathcal{P}}_h^{TH}$ as:

$$\hat{\mathcal{P}}_h^{TH} := \text{span}\,\{R_i^{p,p} \mid i = 1,\dots,n_{\mathcal{P}}^{TH}\}, \tag{23}$$

where

$$n_{\mathcal{P}}^{TH} := \dim(\hat{\mathcal{P}}_h^{TH}) = m \times n. \tag{24}$$

The Taylor–Hood isogeometric spaces in the physical domain are:

$$\begin{cases} \mathcal{V}_{h,0}^{TH} & := \text{span}\{\phi_i^{k,TH} := \mathfrak{e}_k R_i^{p+1,p+1} \circ \mathbf{F}^{-1} \mid i = 1,\dots,n_{V,k}^{TH}; k = 1,2\}, \\ \mathcal{P}_h^{TH} & := \text{span}\{\rho_i^{TH} := R_i^{p,p} \circ \mathbf{F}^{-1} \mid i = 1,\dots,n_{\mathcal{P}}^{TH}\}. \end{cases} \tag{25}$$

We will also consider the pressure space as:

$$\mathcal{P}_{h,0}^{TH} := \{p \in \mathcal{P}_h^{TH} \mid \int_\Omega p \, d\Omega = 0\}. \tag{26}$$

3.2. Raviart–Thomas

The Raviart–Thomas (RT) NURBS spaces are described as:

$$\begin{cases} \hat{\mathcal{V}}_h^{RT} & := \hat{\mathcal{N}}_{\alpha_1+1,\alpha_2}^{p+1,p} \times \hat{\mathcal{N}}_{\alpha_1,\alpha_2+1}^{p,p+1}, \\ \hat{\mathcal{P}}_h^{RT} & := \hat{\mathcal{N}}_{\alpha_1,\alpha_2,}^{p}, \end{cases} \tag{27}$$

The $\hat{\mathcal{V}}_h^{RT}$ space is spanned by:

$$\hat{\mathcal{V}}_h^{RT} := \text{span}\,\{\mathfrak{e}_k R_{\alpha+\mathfrak{e}_k,i,j}^{p+\mathfrak{e}_k} \mid i = 1,\dots,n; j = 1,\dots,m; k = 1,2\}, \tag{28}$$

For the constraint discrete velocity space, we will also assume that:

$$\hat{\mathcal{V}}_{h,0}^{RT} := \{\hat{\mathbf{v}}_h \in \hat{\mathcal{V}}_h^{RT} \mid \hat{\mathbf{v}}_h \cdot \mathbf{n} = 0 \text{ on } \partial\hat{\Omega}\}, \tag{29}$$

where $\mathfrak{e}_k$ is the kth canonical basis vector of $\mathbb{R}^2$, and $\hat{\mathcal{V}}_{h,0}^{RT}$ is then spanned by:

$$\hat{\mathcal{V}}_{h,0}^{RT} := \text{span}\{\mathfrak{e}_k R_{\alpha+\mathfrak{e}_k,i,j}^{p+\mathfrak{e}_k} \mid i = 2,\dots,n-1; j = 2,\dots,m-1; k = 1,2\}. \tag{30}$$

The velocity space $\hat{\mathcal{V}}_{h,0}^{RT}$ is rewritten as:

$$\hat{\mathcal{V}}_{h,0}^{RT} := \text{span}\{\varepsilon_k R_{\alpha+\varepsilon_k,i}^{p+\varepsilon_k} \mid i = 1,\ldots,n_{V,k}^{RT}; k = 1,2\}, \tag{31}$$

where:

$$n_{V,1}^{RT} = (n-2)m,\ n_{V,2}^{RT} = n(m-2)\,, \tag{32}$$

as $\hat{\mathcal{P}}_h^{RT} = \hat{\mathcal{P}}_h^{TH}$, the basis for $\hat{\mathcal{P}}_h^{RT}$ is (23) and its dimension is denoted by $n_{\mathcal{P}}^{RT} = n_{\mathcal{P}}^{TH} = n_{\mathcal{P}}$. The Raviart–Thomas isogeometric spaces in the physical domain are:

$$\begin{cases} \mathcal{V}_{h,0}^{RT} := \text{span}\left\{\phi_i^{k,RT} := \left((\det(J_F))^{-1} J_G \varepsilon_k R_{\alpha+\varepsilon_k,i}^{p+\varepsilon_k}\right) \circ \mathbf{F}^{-1} \mid i = 1,\ldots,n_{V,k}^{RT}; k = 1,2\right\}, \\ \mathcal{P}_h^{RT} := \text{span}\left\{\rho_i^{RT} := \left((\det(J_F))^{-1} R_{\alpha,i}^{p,p}\right) \circ \boldsymbol{F}^{-1} \mid i = 1,\ldots,n_{\mathcal{P}}^{RT}\right\}, \end{cases} \tag{33}$$

we used a Piola transform, such as a push-forward for $\mathcal{V}_{h,0}^{RT}$, to assure inf-sup stability [1]. We also consider, in the case of our problem, the pressure space as:

$$\mathcal{P}_{h,0}^{RT} := \{q \in \mathcal{P}_h^{RT} \mid \int_\Omega q\, d\Omega = 0\}. \tag{34}$$

3.3. Nédélec Spaces

The Nédélec (NL) NURBS spaces are defined as:

$$\begin{cases} \hat{\mathcal{V}}_h^N := \hat{\mathcal{N}}_{\alpha+1,\alpha}^{p+1,p+1} \times \hat{\mathcal{N}}_{\alpha,\alpha+1}^{p+1,p+1}, \\ \hat{\mathcal{P}}_h^N := \hat{\mathcal{N}}_{\alpha,\alpha}^{p,p}, \end{cases} \tag{35}$$

For the constraint discrete velocity space, we will also assume that:

$$\hat{\mathcal{V}}_{h,0}^{NL} := \{\hat{\mathbf{v}}_h \in \hat{\mathcal{V}}_h^{NL} \mid \hat{\mathbf{v}}_h = 0 \text{ on } \partial\hat{\Omega}\}, \tag{36}$$

The $\hat{\mathcal{V}}_h^{NL}$ space is spanned by:

$$\hat{\mathcal{V}}_h^{NL} := \text{span}\{\varepsilon_k R_{\boldsymbol{\alpha}+\varepsilon_k,i,j}^{p+1,p+1} \mid i = 1,\ldots,n; j = 1,\ldots,m; k = 1,2\}, \tag{37}$$

where ε_k is the kth canonical basis vector of $\mathbb{R}^2$, and the space $\hat{\mathcal{V}}_{h,0}^{RT}$ is then spanned by:

$$\hat{\mathcal{V}}_{h,0}^{NL} := \text{span}\{\varepsilon_k R_{\boldsymbol{\alpha}+\varepsilon_k,i,j}^{p+1,p+1} \mid i = 2,\ldots,n-1; j = 2,\ldots,m-1; k = 1,2\}, \tag{38}$$

For simplicity of notation, we rewrite $\hat{V}_{h,0}^{NL}$ as:

$$\hat{\mathcal{V}}_{h,0}^{NL} := \text{span}\{\varepsilon_k R_{\boldsymbol{\alpha}+\varepsilon_k,i}^{p+1,p+1} \mid i = 1,\ldots,n_{V,k}^{NL}; k = 1,2\}, \tag{39}$$

where $n_{V,1}^{NL} = n_{V,2}^{NL} := (n-2)(m-2)$.

The pressure space $\hat{\mathcal{P}}_h^{NL}$ is represented as:

$$\hat{\mathcal{P}}_h^{NL} := \text{span}\{R_{i,j}^{p,p} \mid i = 1,\ldots,n; j = 1,\ldots,m; k = 1,2\}, \tag{40}$$

By using a similar notation to the above, we write $\hat{\mathcal{P}}_h^{NL}$ as:

$$\hat{\mathcal{P}}_h^{NL} := \text{span}\{R_i^{p,p} \mid i = 1,\ldots,\mathcal{P}_n^{NL}\}, \tag{41}$$

where:

$$\mathcal{P}_n^{NL} := \dim\left(\hat{\mathcal{P}}_h^{NL}\right) = nm. \tag{42}$$

The Nédélec isogeometric spaces in the physical domain are:

$$\begin{cases} \mathcal{V}_{h,0}^{NL} & := \text{span}\{\phi_i^{k,NL} := \varepsilon_k R_{\boldsymbol{\alpha}+\varepsilon_k,i}^{p+1,p+1} \circ \mathbf{F}^{-1} \mid i = 1,\ldots,n_{V,k}^{NL}; k = 1,2\}, \\ \mathcal{P}_h^{NL} & := \text{span}\{\rho_i^{NL} := R_i^{p,p} \circ \mathbf{F}^{-1} \mid i = 1,\ldots,\mathcal{P}_n^{NL}\}. \end{cases} \tag{43}$$

We will also consider the pressure space as:

$$\mathcal{P}_{h,0}^{NL} := \{q \in \mathcal{P}_h^{NL} \mid \int_\Omega q \, d\Omega = 0\}. \tag{44}$$

4. The Brinkman Problem

4.1. Formulation Variation of the Brinkman Problem

Let $\Omega \subset \mathbb{R}^2$ be bounded open, given by the NURBS parameterization $\mathbf{F}$, and $\Gamma = \Gamma_D \cup \Gamma_N$ ($\Gamma_D \cap \Gamma_N = \varnothing$), with Γ defined by the $\mathbf{F}$-image of collection of faces of $\hat{\Omega}$. The Brinkman equations explain the flow through a porous medium presented by the system.

$$\begin{cases} -\widetilde{\mu}\Delta u + \nabla p + \mu\kappa^{-1}u &= f, \quad \text{in } \Omega, \\ \nabla \cdot u &= 0, \quad \text{in } \Omega, \end{cases} \tag{45}$$

This is subject to the boundary conditions:

$$\begin{cases} u &= h, \text{ on } \Gamma_D, \\ \widetilde{\mu}\frac{\partial u}{\partial n} - pn &= g, \text{ on } \Gamma_N. \end{cases} \tag{46}$$

In these equations, p and v represent the pressure and velocity fields, respectively. with p belonging to the space $L^2(\Omega)$. We assume that f is a given source $\left(f \in \left[L^2(\Omega)\right]^2\right)$. The fluid under consideration defined by the Newtonian fluid viscosity, the functions $\widetilde{\mu} \in L^\infty(\Omega)$, and the physical dynamic viscosity $\mu \in L^\infty(\Omega)$. We impose a null mean value of the pressure field p over the entire domain Ω to assure the uniqueness of p, i.e.,

$$\int_\Omega p \, dx = 0, \tag{47}$$

κ^{-1} presents the permeability of the reservoir. To guarantee the existence of the weak solution, we assume that there exist two constants, $k_1, k_2 \succ 0$, such that κ^{-1} is a tensor satisfying the following inequality:

$$k_1\psi^t\psi \leq \psi^t\kappa^{-1}\psi \leq k_2\psi^t\psi, \ \forall\psi \in \mathbb{R}^2, \tag{48}$$

and we assume that $(g,h) \in \left[L^2(\Gamma_N)\right]^2 \times \left[L^2(\Gamma_D)\right]^2$. Using, $H_0^1(\Omega)$ we determine that the subspace of the standard Sobolev space $H^1(\Omega)$ makes all functions vanish on the boundary $\partial\Omega = \Gamma$. We present

$$X = \left[H^1(\Omega) : \ u = h\right]^2, \tag{49}$$

as the velocity space and

$$M = \{q \in L^2(\Omega), \int_\Omega q dx = 0\}, \tag{50}$$

as the pressure space.

The weak formulation of the Brinkman system (45)–(47) enables us to find $(u,p) \in X \times M$, such that:

$$\begin{cases} a(u,v)+b(v,p) &= F(v), \quad \forall v \in X, \\ b(q,u) &= 0, \quad \forall q \in M, \end{cases} \tag{51}$$

where $a(\cdot,\cdot)$ and $b(\cdot,\cdot)$ are the bilinear forms defined by:

$$\begin{cases} a(u,v) = \int_\Omega \widetilde{\mu}\nabla u \nabla v dx + \int_\Omega \mu\kappa^{-1} u.v dx, \\ b(v,p) = -\int_\Omega p\nabla.v dx, \end{cases} \tag{52}$$

and $F : X \to \mathbb{R}$ is the continuous function:

$$F(v) = \int_\Omega f.v dx + \int_{\Gamma_N} g.v d\sigma, \tag{53}$$

We equip the spaces M, $L^2(\Omega)$, X and $X \times M$ with the norms

$$\| v \|_{0,\Omega} := \| v \|_M = \| v \|_{L^2(\Omega)} = \left(\int_\Omega |v|^2 dx \right)^{\frac{1}{2}} \forall v \in L^2(\Omega), \tag{54}$$

$$\| v \|_1^2 := \| \nabla v \|_{0,\Omega}^2 + \| v \|_{0,\Omega}^2, \tag{55}$$

$$\| v \|_X := a(v,v)^{\frac{1}{2}}, \tag{56}$$

and

$$\| (v,q) \|_{X\times M} := \| v \|_X + \| q \|_M, \tag{57}$$

Theorem 1. *Problem (51) has a unique weak solution* $(u,p) \in X \times M$.

4.2. Approximate Formulation of the Brinkman Problem

In its original form, IGA entails using a Galerkin formulation and a finite-dimensional subspace of X that is spanned by the same set of B-Splines/NURBS basis functions as those characterizing the geometry used to find an approximate solution to (45) and (46). As a result, we present the functional spaces $X_h = \mathcal{V}_h(\Omega) \cap X$ and $M_h = \mathcal{P}_h(\Omega) \cap M$. Where $\mathcal{V}_h$ and $\mathcal{P}_h$ are defined using multivariate NURBS functions that were introduced in Section 3. The IGA formulation then reads: Find $(u_h, p_h) \in X_h \times M_h$ such that:

$$\begin{cases} a(u_h,v_h)+b(v_h,p_h) &= f(v_h), \quad \forall v_v \in X_h, \\ b(q_h,u_h) &= 0, \quad \forall q_h \in M_h, \end{cases} \tag{58}$$

To define the corresponding linear algebraic system, we use a set of vector-valued basis functions $\{N_i\}_{i=1}^{n_u}$ and $\{N_j\}_{j=1}^{n_p}$ for the spaces X_h and M_h, respectively, so that:

$$u_h = \sum_{i=1}^{n_u} N_i u_i, \; p_h = \sum_{j=1}^{n_p} N_j p_j, \tag{59}$$

where n_u and n_p are the dimensions of the discrete spaces of velocity X_h and of pressure M_h, respectively.

By using the bilinear proprieties of $a(.,.)$ and $b(.,.)$, we obtain the linear system:

$$\begin{bmatrix} A & B^t \\ B & 0 \end{bmatrix} \begin{bmatrix} u \\ p \end{bmatrix} = \begin{bmatrix} F \\ 0 \end{bmatrix}, \tag{60}$$

where $A = [a(N_i, N_k)]_{i,k=1}^{n_u}$, $B = \left[b(N_i, N_j)\right]_{i,j=1}^{n_u,n_p}$, $u = [u_i]_{i=1}^{n_u}$, $p = \left[p_j\right]_{j=1}^{n}$, and $F = [f(N_i)]_{i=1}^{n}$.

5. Numerical Results

In this section, we perform numerical verification of our chosen elements using two example tests with exact solutions, with the first one in a square domain and the second one in an annulus domain. Then, we solve our problem for two-dimensional flow and represent well-established benchmark problems, for which we compare the results between the three families of elements studied in this paper.

We want to highlight that, in the NURBS-based IGA framework, the two-dimensional lid-driven flow in a quarter of an annulus benefits from the exact geometric representation provided by NURBS. This is in contrast to standard FE methods. For numerical simulation in Matlab, based on the IGA library GeoPDEs [43], the regularity α is assumed equal to $p-1$.

The graphs of the error are presented on a log–log scale, and in this work, the L^2 error and H^1 error are defined as:

$$\| e_h \|_{L^2} = \left(\int_\Omega |u_h - u|^2 d\Omega \right)^{\frac{1}{2}}, \tag{61}$$

$$\text{and} \quad \| e_h \|_{H^1} = \left(\int_\Omega \left(|u_h - u|^2 + |\nabla u_h - \nabla u|^2 \right) d\Omega \right)^{\frac{1}{2}}, \tag{62}$$

where u is an exact solution and u_h is an approximated solution to our problem.

We use the following formula:

$$r_{(\cdot)} = \log_2 \left(\frac{\| e_h \|_{(\cdot)}}{\| e_{h/2} \|_{(\cdot)}} \right), \tag{63}$$

where $(\cdot)$ defines the L^2- or H^1-norm, to demonstrate the convergence rate.

5.1. The Brinkman Problem on the Unit Square

In order to test the accuracy and reliability of the compatible spaces considered, in this first example, we consider the parametric domain $\hat{\Omega} = \Omega = (0,1) \times (0,1)$, by using the manufactured solution presented in [26]. The exact velocity u and exact pressure p of the Brinkman system (45) and (46) are given below,

$$u = \begin{pmatrix} 2\cos(\pi y)\sin(\pi y)\sin(\pi x)^2 \\ -2\cos(\pi x)\sin(\pi x)\sin(\pi y)^2 \end{pmatrix}, \text{ and } p = \cos(\pi x)\cos(\pi y), \tag{64}$$

it is easy to check that $\nabla \cdot u = 0$ and $\int_\Omega p = 0$. $\tilde{\mu} = \mu = 1$, with the highly varying permeability κ^{-1} equal to $\kappa^{-1} = a(\sin(\pi x) + 1.1)$, where a is a given constant. The values of κ^{-1} are plotted in Figure 2 for $a = 10^{-4}$. The boundary conditions considered in this test are:

$$u = o, \text{ on } \Gamma = \Gamma_D \tag{65}$$

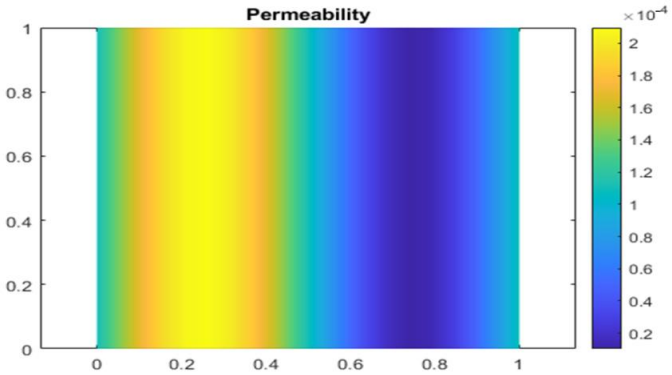

Figure 2. Permeability.

The vector fields and pressure contours corresponding IGA solutions in three types of element spaces are presented in Figures 3 and 4, with the domain discretized using a 16×32 mesh.

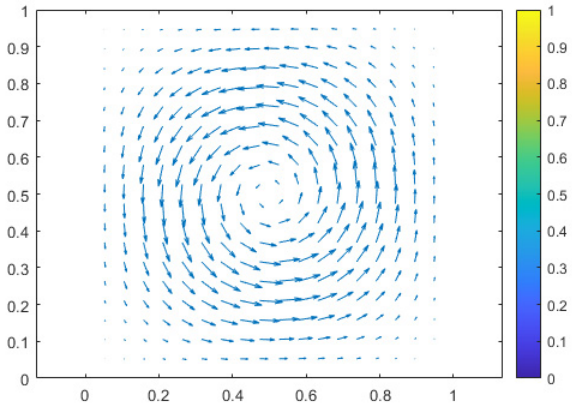

(**a**)

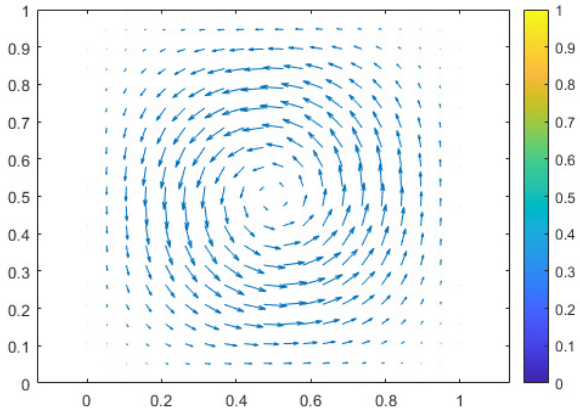

(**b**)

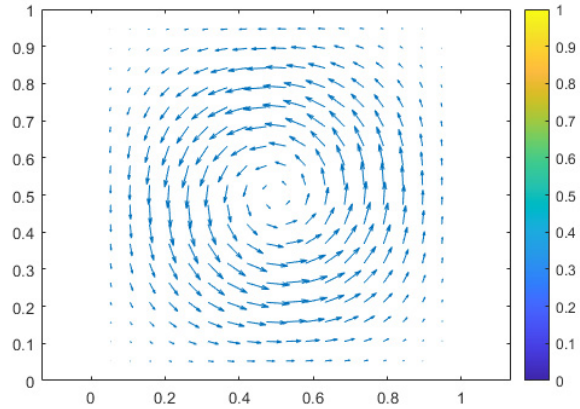

(c)

Figure 3. Vector fields of approximate solutions for three families: approximate NDL solution (**a**), approximate RT solution (**b**), approximate TH solution (**c**).

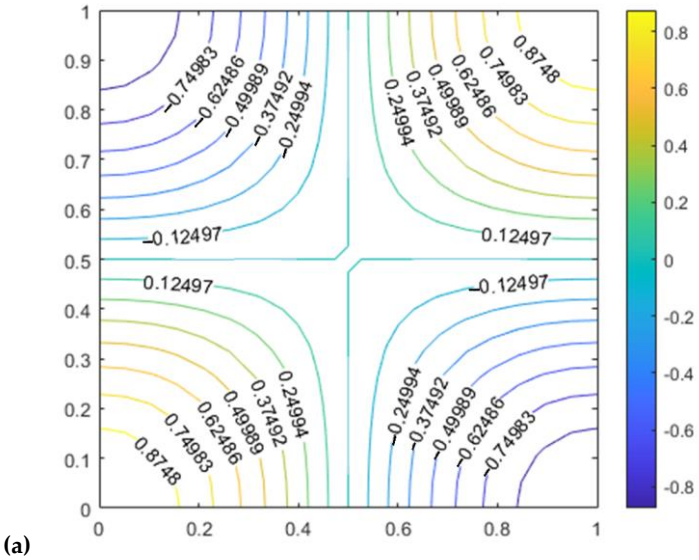

(a)

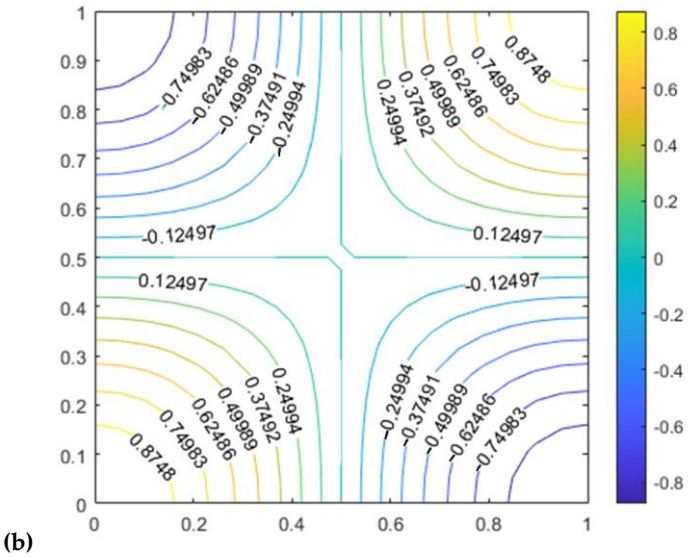

(b)

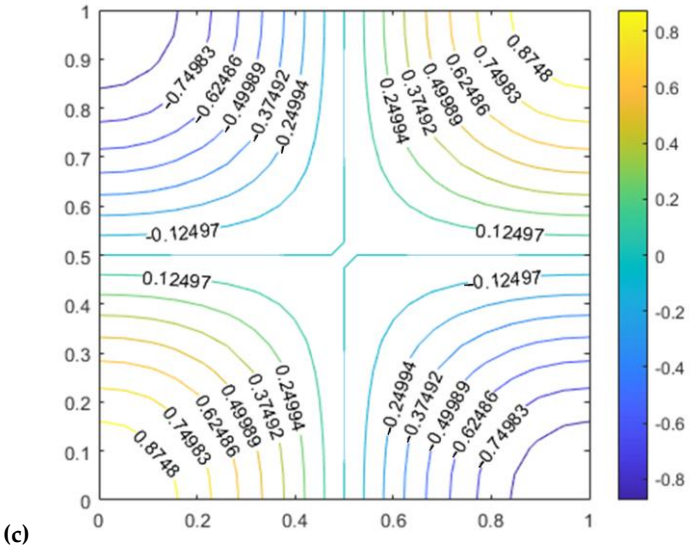

(c)

Figure 4. Pressure contours of approximate solutions for three families: approximate NDL solution (**a**), approximate RT solution (**b**), approximate TH solution (**c**).

In this paragraph, using the data from the example provided in Section 5.1, we investigate the convergence of the discrete formulation for the three families of mixed elements under discussion.

Figure 5: For p, the degree of the pressure space is equal to 2 (a), (b), and (c), showing the velocity L^2 errors, the velocity H^1 errors, and the L^2 error of the pressure field, respectively. Similar to this, we examine the three mixed elements under discussion with degrees of p = 3 and p = 4. Figures 6 and 7 demonstrate comparable results. The results were obtained with different consecutive mesh dimensions: 4 × 4; 8 × 8; 16 × 16; and 32 × 32.

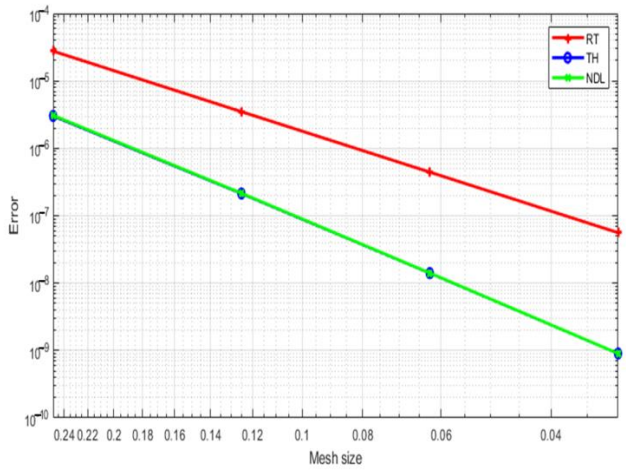

(a)

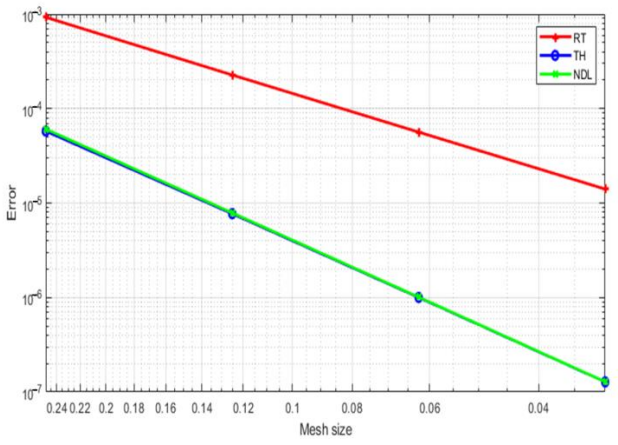

(b)

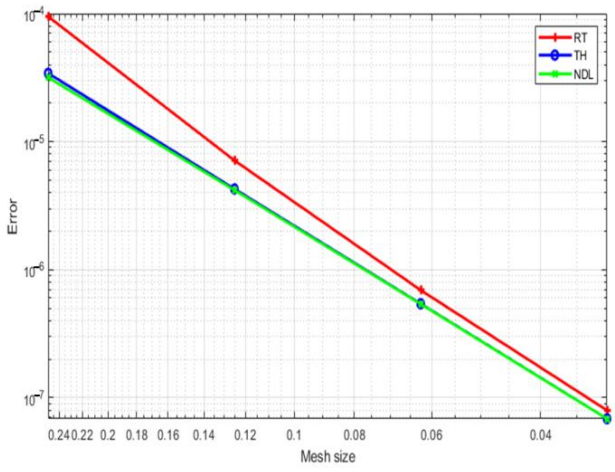

(c)

Figure 5. Velocity field L^2 errors (**a**), velocity field H^1 errors (**b**), and the pressure field L^2 error (**c**) with p = 2.

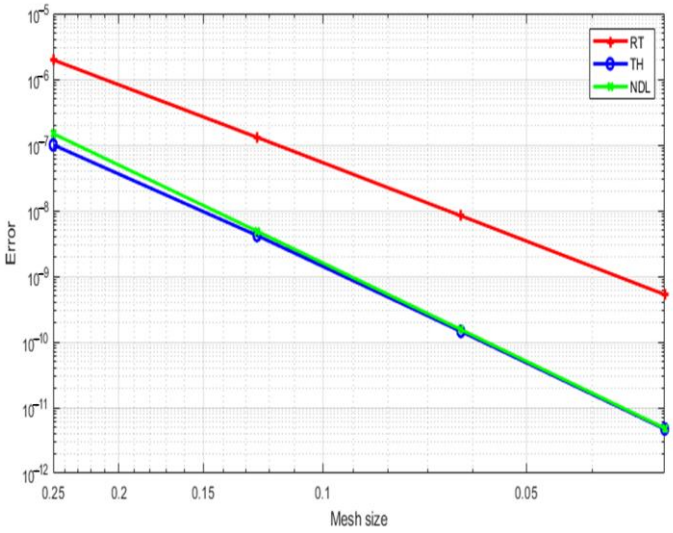

(a)

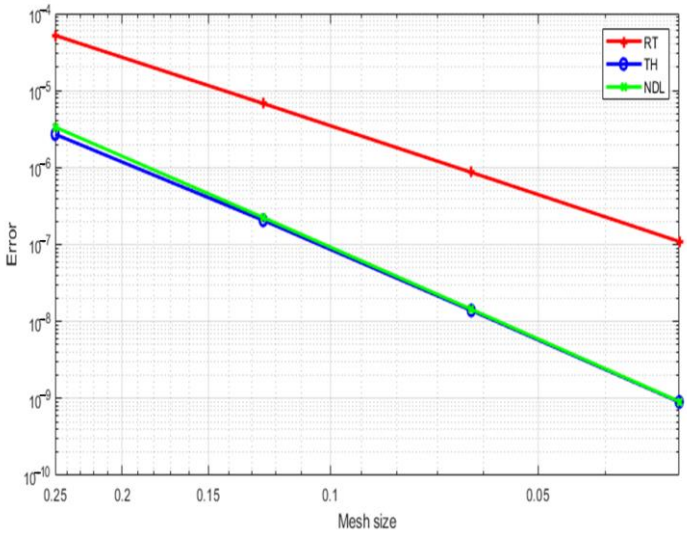

(b)

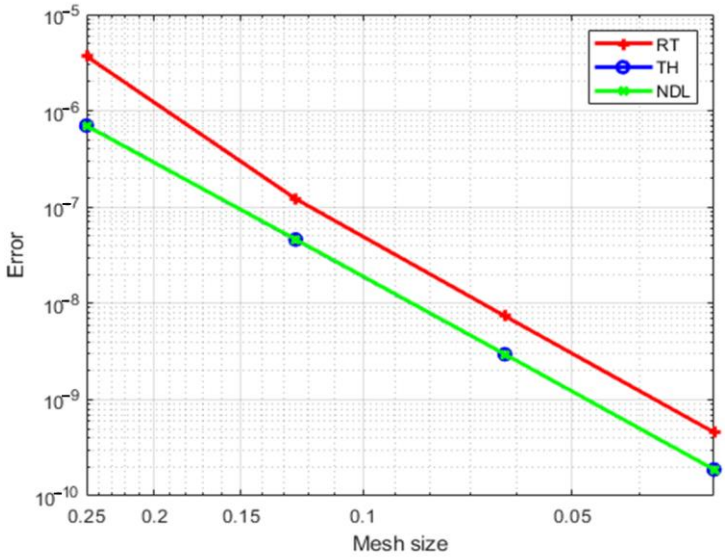

(c)

Figure 6. Velocity field L^2 errors (**a**), velocity field H^1 errors (**b**), and the pressure field L^2 error (**c**) with p = 3.

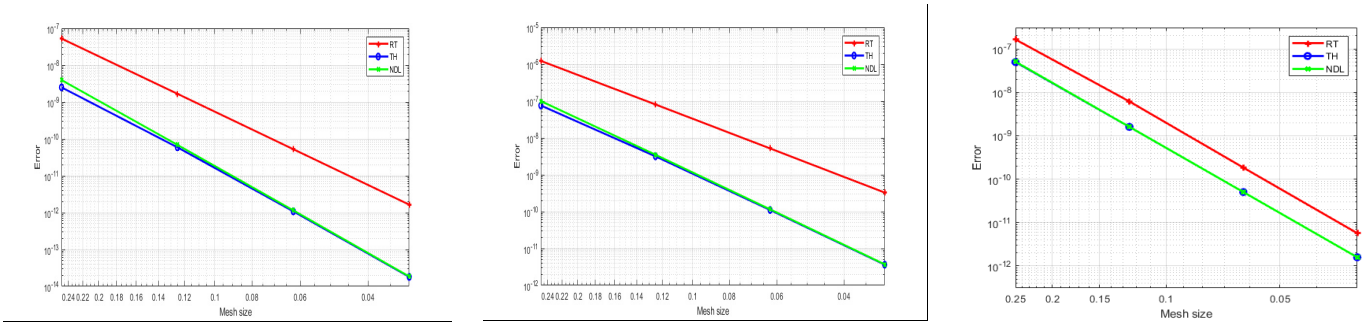

(**a**) (**b**) (**c**)

Figure 7. Velocity field L^2 errors (**a**), velocity field H^1 errors (**b**), and the pressure field L^2 error (**c**) with p = 4.

5.2. The Brinkman Problem on a NURBS Surface

Now that we have tested the approach on a parametric domain $\hat{\Omega}$, we want to test it on a physical domain Ω. Let the first quadrant be part of an annulus with inner radius r = 1 and outer radius R = 4 that is centered at the origin and is represented in polar coordinates by the inequalities $1 < r < 4$ and $0 < \theta < \pi/2$; the domain is described in Figure 8.

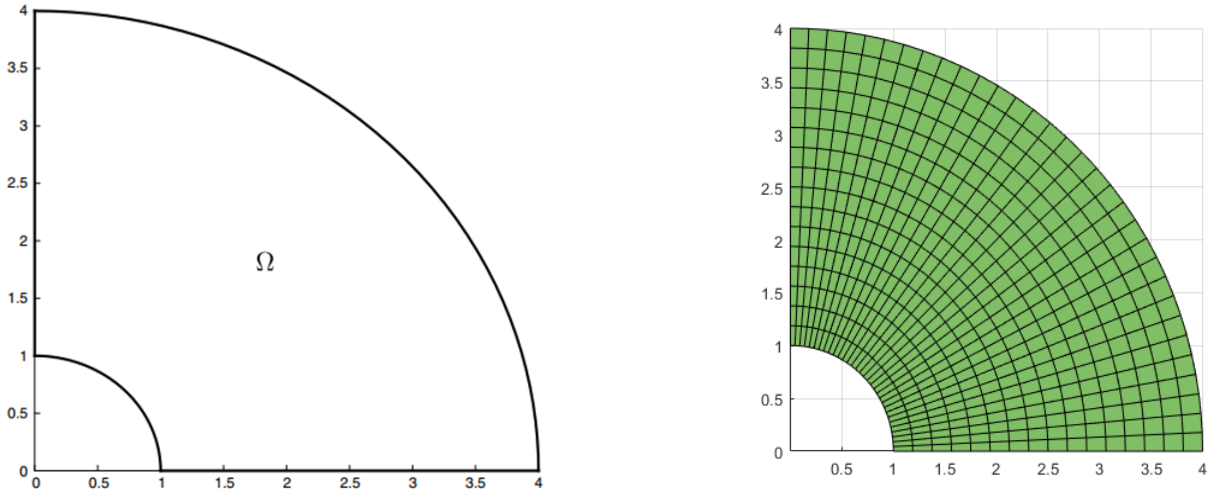

(**a**) (**b**)

Figure 8. Geometry of a quarter-ring (**a**), with the mesh of its NURBS represented as 16×32 (**b**).

In order to obtain a manufactured solution to systems (45) and (46), we consider a potential function φ such as:

$$u = \begin{bmatrix} \frac{\partial \varphi}{\partial y} \\ -\frac{\partial \varphi}{\partial x} \end{bmatrix}, \tag{66}$$

where u is our exact velocity solution. It is easy to show that u satisfies the incompressibility condition div, $u = 0$. Using polar coordinates, here, we choose the potential function:

$$\varphi(r, \theta) = (r-1)^2(4-r)^2(1-\cos 4\theta\ ), \tag{67}$$

which gives, in Cartesian coordinates:

$$\varphi(x, y) = 8x^2y^2\left(1 - \frac{1}{\sqrt{x^2+y^2}}\right)^2\left(\frac{4}{\sqrt{x^2+y^2}} - 1\right)^2. \tag{68}$$

For the boundary condition, we assume that $u|_{\Gamma_D} = 0$ ($\partial\Omega = \Gamma_D$ *and* $\Gamma_N = \varnothing$). The other problem data are defined as follows:

$$\tilde{\mu} = \mu = 1, \ \kappa^{-1} = a(\sin(\pi x) + 1.1), \tag{69}$$

The constant $a = 0.0001$. Figure 9 presents the dstribution of the permeability κ^{-1}, with the pressure p chosen to have an average of zero on Ω. Here, we use $p = (4 - y)x$, and the right-hand side is calculated as $-\nabla \cdot (\tilde{\mu}\nabla u) + \nabla p + \mu\kappa^{-1}u = f$. The vector fields and pressure contours, corresponding the IGA solutions to three types of element spaces, are presented in Figures 10 and 11, with the domain discretized using a 16×32 mesh.

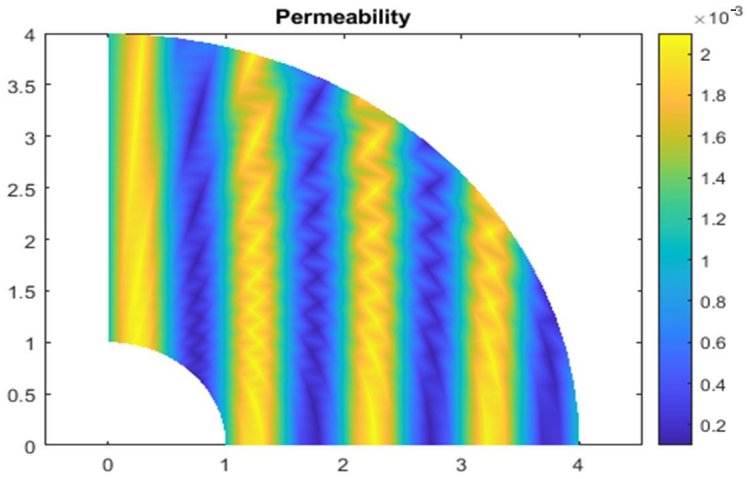

Figure 9. Permeability.

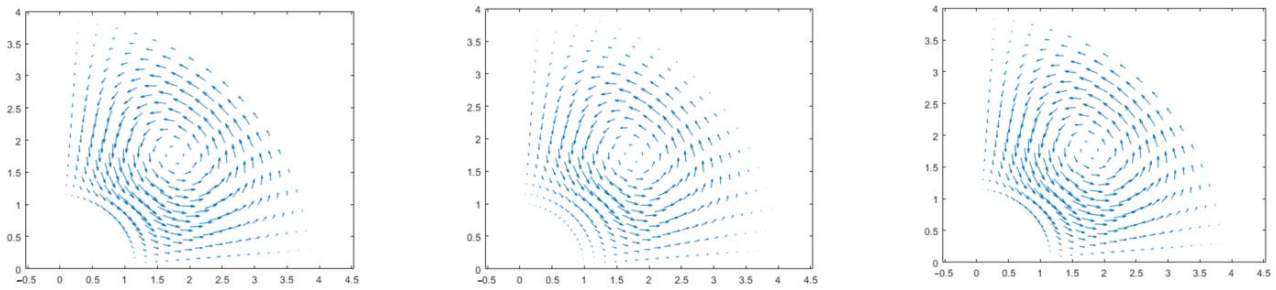

(**a**) (**b**) (**c**)

Figure 10. Vector fields of approximate solution for three families: NDL (**a**), approximate RT solution (**b**), approximate TH solution (**c**).

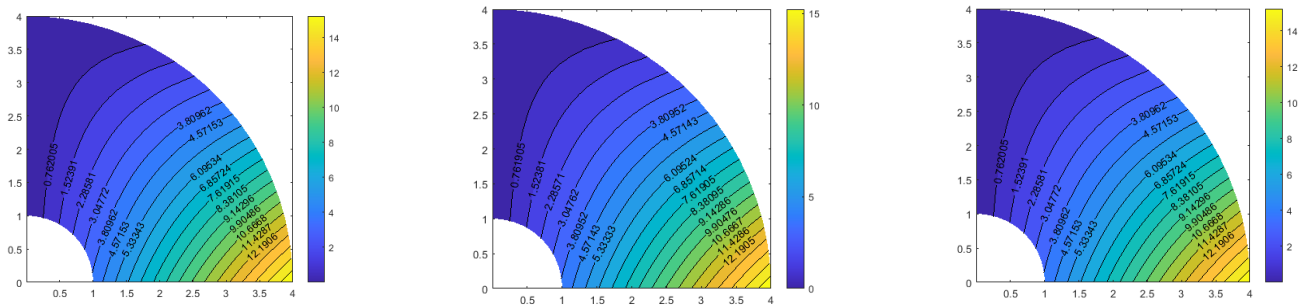

(**a**) (**b**) (**c**)

Figure 11. Pressure contours of approximate solution for three families: NDL (**a**), approximate RT solution (**b**), approximate TH solution (**c**).

In this paragraph, using the data from the example provided in Section 5.1, we investigate the convergence of the discrete formulation for the three families of mixed elements under discussion.

Figure 12: For p, the degree of the pressure space is equal to 2 (a), (b), and (c), showing velocity L^2-errors, velocity H^1-errors, and the L^2-errors in the pressure field, respectively. Similar to this, we examine the three mixed elements under discussion with degrees of p = 3 and p = 4. Figures 13 and 14 demonstrate comparable results. Our results were obtained with different consecutive mesh dimensions: 4×8; 8×16; 16×32; and 32×64.

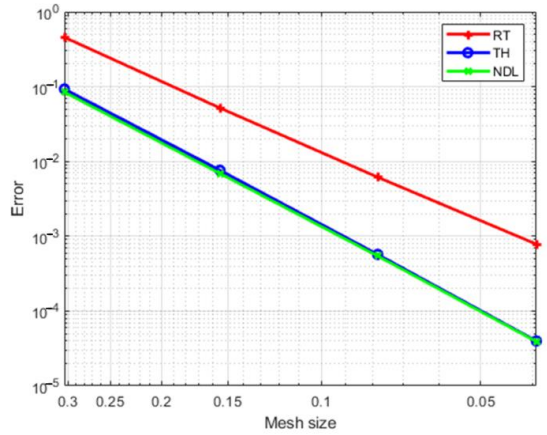

(a)

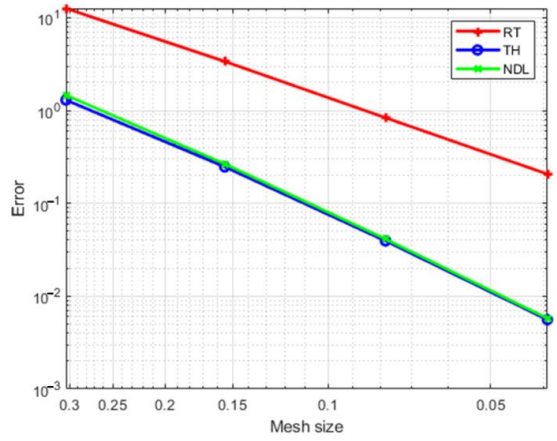

(b)

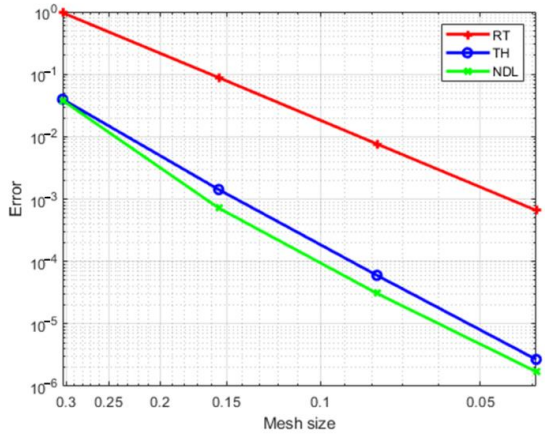

(c)

Figure 12. Velocity field L^2 errors (**a**), velocity field H^1 errors (**b**), and the pressure field L^2 errors (**c**) for quarter of an annulus with p = 2.

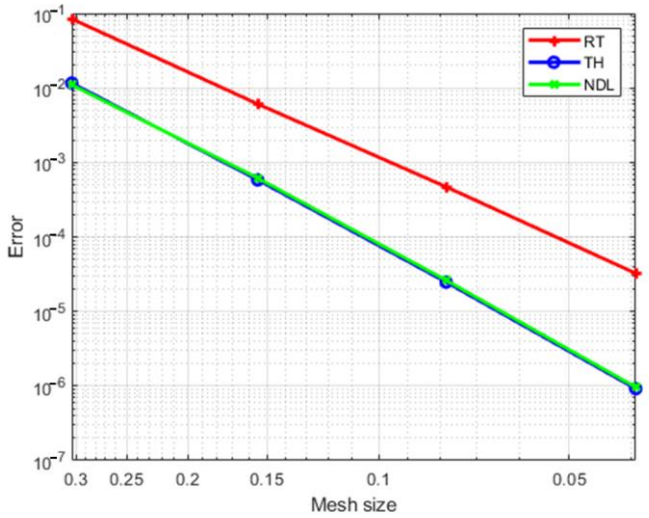

(a)

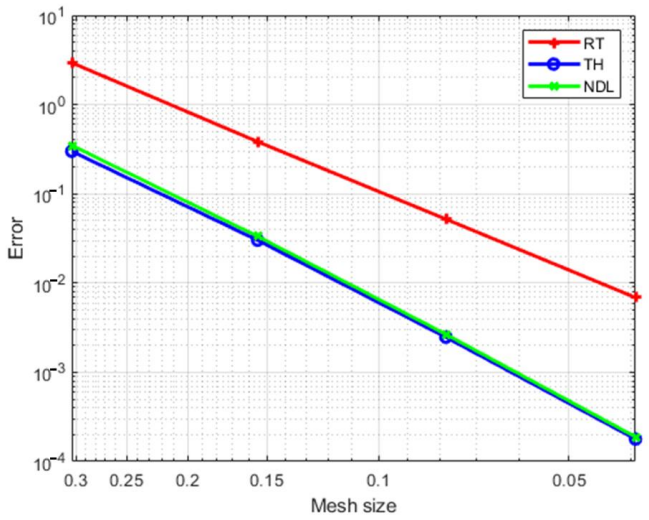

(b)

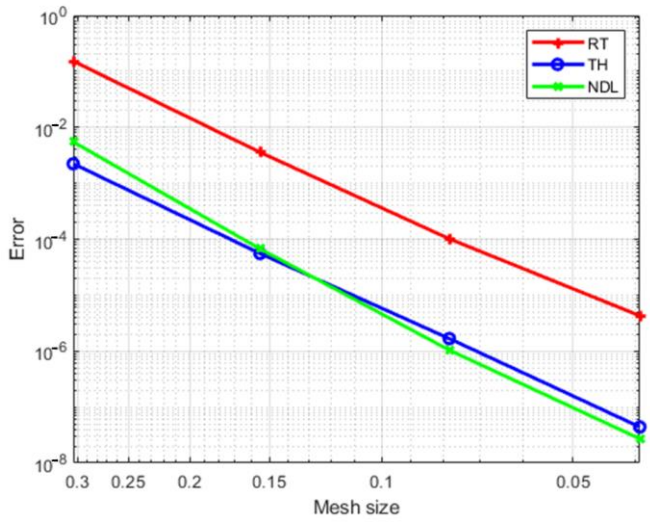

(c)

Figure 13. Velocity field L^2 errors (**a**), velocity field H^1 errors (**b**), and the pressure field L^2 errors (**c**) for quarter of an annulus with p = 3.

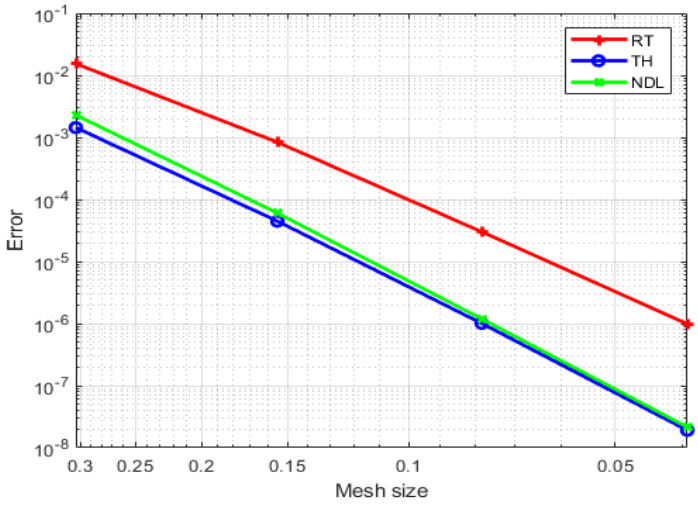

(a)

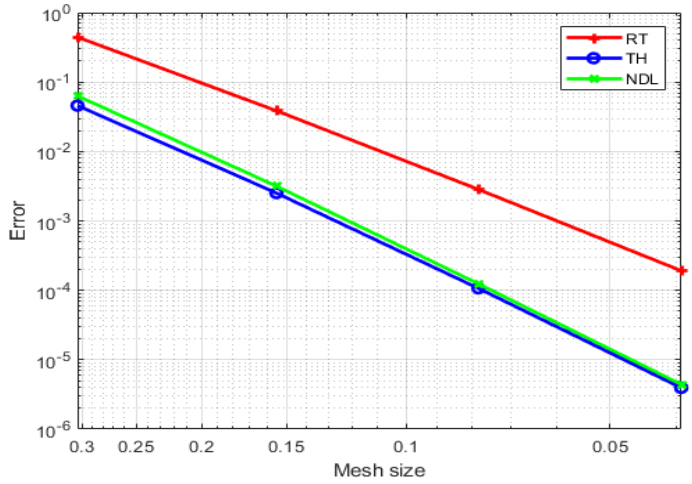

(b)

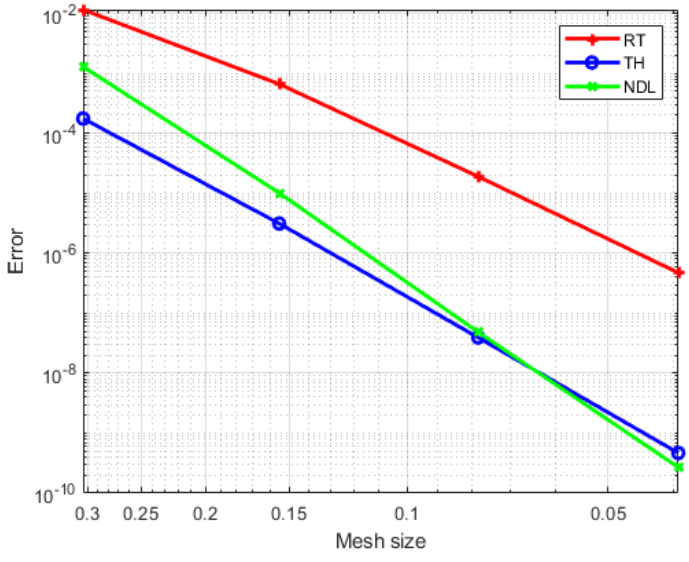

(c)

Figure 14. Velocity field L^2 errors (**a**), velocity field H^1 errors (**b**), and the pressure field L^2 error (**c**) for quarter of an annulus with p = 4.

6. Conclusions

In this paper, we focus on the Brinkman system and investigate the performance of three well-established isogeometric discretizations that are known to be stable and converge toward the Stokes problem. These discretizations include an extension of the inf-sup stable Taylor–Hood element, as described in [1,3]; an extension of the Raviart–Thomas element, which is stable and preserves the structure by ensuring pointwise divergence-free discrete solutions, as described in [3]; and an extension of the inf-sup stable Nédélec element, as described in [2]. For two generic test cases corresponding to a domain of a square $(0,1) \times (0,1)$ and a quarter ring, we evaluated the convergence behavior of the three families of elements in the case of mesh refinement for quadratic, cubic, and quartic approximations. An extension of the study described in this article will be presented in a future article on the multi-patch NURBS domain.

Author Contributions: Conceptualization, L.E.O., O.E.M., A.E.A. and A.E.; Methodology, A.E.A. and A.E.; Validation, L.E.O., O.E.M., A.E.A., S.V. and M.L.S.; Formal analysis, L.E.O., A.E.A., S.V. and M.L.S.; Investigation, L.E.O., O.E.M., A.E.A. and A.E.; Resources, A.E.; Data curation, L.E.O., O.E.M. and M.L.S.; Writing—original draft, L.E.O., O.E.M., A.E.A. and A.E.; Writing—review & editing, S.V. and M.L.S.; Visualization, L.E.O., O.E.M., A.E.A., A.E., S.V. and M.L.S.; Supervision, A.E.A., A.E., S.V. and M.L.S.; Funding acquisition, M.L.S. All authors have read and agreed to the published version of the manuscript.

Funding: This research received no external funding.

Data Availability Statement: The data associated with this research are available upon request.

Conflicts of Interest: The authors declare no conflict of interest.

References

1. Buffa, A.; De Falco, C.; Sangalli, G. Isogeometric Analysis: Stable Elements for the 2D Stokes Equation. *Int. J. Numer. Methods Fluids* **2011**, *65*, 1407–1422.
2. Bressan, A.; Sangalli, G. Isogeometric Discretizations of the Stokes Problem: Stability Analysis by the Macroelement Technique. *IMA J. Numer. Anal.* **2013**, *33*, 629–651. [CrossRef]
3. Evans, J.A.; Hughes, T.J.R. Isogeometric Divergence-Conforming b-Splines for the Darcy–Stokes–Brinkman Equations. *Math. Model. Methods Appl. Sci.* **2013**, *23*, 671–741. [CrossRef]
4. Hughes, T.J.; Cottrell, J.A.; Bazilevs, Y. Isogeometric Analysis: CAD, Finite Elements, NURBS, Exact Geometry and Mesh Refinement. *Comput. Methods Appl. Mech. Eng.* **2005**, *194*, 4135–4195.
5. Cottrell, J.A.; Hughes, T.J.; Bazilevs, Y. *Isogeometric Analysis: Toward Integration of CAD and FEA*; John Wiley & Sons: Hoboken, NJ, USA, 2009.
6. De Boor, C.; De Boor, C. *A Practical Guide to Splines*; Springer-Verlag: New York, NY, USA, 1978; Volume 27.
7. El Fakkoussi, S.; Moustabchir, H.; Elkhalfi, A.; Pruncu, C.I. Computation of the Stress Intensity Factor KI for External Longitudinal Semi-Elliptic Cracks in the Pipelines by FEM and XFEM Methods. *Int. J. Interact. Des. Manuf.* **2019**, *13*, 545–555.
8. Łoś, M.M.; Woźniak, M.; Paszyński, M.; Lenharth, A.; Hassaan, M.A.; Pingali, K. IGA-ADS: Isogeometric Analysis FEM Using ADS Solver. *Comput. Phys. Commun.* **2017**, *217*, 99–116. [CrossRef]
9. Piegl, L.; Tiller, W. *The NURBS Book*; Springer Science & Business Media: Berlin/Heidelberg, Germany, 1996.
10. Yakoubi, K.; Montassir, S.; Moustabchir, H.; Elkhalfi, A.; Pruncu, C.I.; Arbaoui, J.; Farooq, M.U. An Extended Finite Element Method (XFEM) Study on the Elastic T-Stress Evaluations for a Notch in a Pipe Steel Exposed to Internal Pressure. *Mathematics* **2021**, *9*, 507. [CrossRef]
11. Babuška, I. The Finite Element Method with Lagrangian Multipliers. *Numer. Math.* **1973**, *20*, 179–192.
12. Brezzi, F. On the Existence, Uniqueness and Approximation of Saddle-Point Problems Arising from Lagrangian Multipliers. In *Publications Mathématiques et Informatique de Rennes*; Université de Rennes: Rennes, France, 1974; pp. 1–26.
13. El Moutea, O.; El Amri, H.; El Akkad, A. Finite Element Method for the Stokes–Darcy Problem with a New Boundary Condition. *Numer. Anal. Appl.* **2020**, *13*, 136–151.
14. El-Mekkaoui, J.; Elkhalfi, A.; Elakkad, A. Resolution of Stokes Equations with the Ca, b Boundary Condition Using Mixed Finite Element Method. *WSEAS Trans. Math.* **2013**, *12*, 586–597.
15. Elakkad, A.; Elkhalfi, A.; Guessous, N. An a Posteriori Error Estimate for Mixed Finite Element Approximations of the Navier-Stokes Equations. *J. Korean Math. Soc.* **2011**, *48*, 529–550.
16. Mardal, K.A.; Tai, X.-C.; Winther, R. A Robust Finite Element Method for Darcy–Stokes Flow. *SIAM J. Numer. Anal.* **2002**, *40*, 1605–1631.

17. Araya, R.; Harder, C.; Poza, A.H.; Valentin, F. Multiscale Hybrid-Mixed Method for the Stokes and Brinkman Equations—The Method. *Comput. Methods Appl. Mech. Eng.* **2017**, *324*, 29–53. [CrossRef]
18. Bernardi, C.; Hecht, F.; Nouri, F.Z. A New Finite-Element Discretization of the Stokes Problem Coupled with the Darcy Equations. *IMA J. Numer. Anal.* **2010**, *30*, 61–93. [CrossRef]
19. Botti, L.; Di Pietro, D.A.; Droniou, J. A Hybrid High-Order Discretisation of the Brinkman Problem Robust in the Darcy and Stokes Limits. *Comput. Methods Appl. Mech. Eng.* **2018**, *341*, 278–310. [CrossRef]
20. Juntunen, M.; Stenberg, R. Analysis of Finite Element Methods for the Brinkman Problem. *Calcolo* **2010**, *47*, 129–147.
21. Burman, E.; Hansbo, P. A Unified Stabilized Method for Stokes' and Darcy's Equations. *J. Comput. Appl. Math.* **2007**, *198*, 35–51. [CrossRef]
22. Cáceres, E.; Gatica, G.N.; Sequeira, F.A. A Mixed Virtual Element Method for the Brinkman Problem. *Math. Model. Methods Appl. Sci.* **2017**, *27*, 707–743. [CrossRef]
23. Di Pietro, D.A.; Droniou, J. A Polytopal Method for the Brinkman Problem Robust in All Regimes. *Comput. Methods Appl. Mech. Eng.* **2023**, *409*, 115981. [CrossRef]
24. Könnö, J.; Stenberg, R. H(Div)-Conforming Finite Elements for the Brinkman Problem. *Math. Model. Methods Appl. Sci.* **2011**, *21*, 2227–2248. [CrossRef]
25. Vacca, G. An H1-Conforming Virtual Element for Darcy and Brinkman Equations. *Math. Model. Methods Appl. Sci.* **2018**, *28*, 159–194. [CrossRef]
26. Zhang, L.; Feng, M.; Zhang, J. A Globally Divergence-Free Weak Galerkin Method for Brinkman Equations. *Appl. Numer. Math.* **2019**, *137*, 213–229. [CrossRef]
27. El Moutea, O.; El Amri, H.; El Akkad, A. Mixed Finite Element Method for Flow of Fluid in Complex Porous Media with a New Boundary Condition. *Comput. Sci.* **2020**, *15*, 413–431.
28. Anaya, V.; Gatica, G.N.; Mora, D.; Ruiz-Baier, R. An Augmented Velocity–Vorticity–Pressure Formulation for the Brinkman Equations. *Int. J. Numer. Methods Fluids* **2015**, *79*, 109–137.
29. Bressan, A. Isogeometric Regular Discretization for the Stokes Problem. *IMA J. Numer. Anal.* **2011**, *31*, 1334–1356. [CrossRef]
30. Buffa, A.; Rivas, J.; Sangalli, G.; Vázquez, R. Isogeometric Discrete Differential Forms in Three Dimensions. *SIAM J. Numer. Anal.* **2011**, *49*, 818–844. [CrossRef]
31. Hoang, T.; Verhoosel, C.V.; Auricchio, F.; van Brummelen, E.H.; Reali, A. Mixed Isogeometric Finite Cell Methods for the Stokes Problem. *Comput. Methods Appl. Mech. Eng.* **2017**, *316*, 400–423. [CrossRef]
32. Bazilevs, Y.; Beirao da Veiga, L.; Cottrell, J.A.; Hughes, T.J.; Sangalli, G. Isogeometric Analysis: Approximation, Stability and Error Estimates for h-Refined Meshes. *Math. Model. Methods Appl. Sci.* **2006**, *16*, 1031–1090.
33. Hosseini, B.S.; Turek, S.; Möller, M.; Palmes, C. Isogeometric Analysis of the Navier–Stokes–Cahn–Hilliard Equations with Application to Incompressible Two-Phase Flows. *J. Comput. Phys.* **2017**, *348*, 171–194. [CrossRef]
34. Nielsen, P.N.; Gersborg, A.R.; Gravesen, J.; Pedersen, N.L. Discretizations in Isogeometric Analysis of Navier–Stokes Flow. *Comput. Methods Appl. Mech. Eng.* **2011**, *200*, 3242–3253. [CrossRef]
35. Aronson, R.M.; Evans, J.A. Divergence-Conforming Isogeometric Collocation Methods for the Incompressible Navier–Stokes Equations. *Comput. Methods Appl. Mech. Eng.* **2023**, *410*, 115990. [CrossRef]
36. Evans, J.A.; Hughes, T.J.R. Isogeometric Divergence-Conforming B-Splines for the Unsteady Navier–Stokes Equations. *J. Comput. Phys.* **2013**, *241*, 141–167. [CrossRef]
37. Hosseini, B.S.; Möller, M.; Turek, S. Isogeometric Analysis of the Navier–Stokes Equations with Taylor–Hood B-Spline Elements. *Appl. Math. Comput.* **2015**, *267*, 264–281. [CrossRef]
38. Rogers, D.F. *An Introduction to NURBS: With Historical Perspective*; Morgan Kaufmann: Burlington, MA, USA, 2001.
39. Bosy, M.; Montardini, M.; Sangalli, G.; Tani, M. A Domain Decomposition Method for Isogeometric Multi-Patch Problems with Inexact Local Solvers. *Comput. Math. Appl.* **2020**, *80*, 2604–2621. [CrossRef]
40. Chan, C.L.; Anitescu, C.; Rabczuk, T. Isogeometric Analysis with Strong Multipatch C1-Coupling. *Comput. Aided Geom. Des.* **2018**, *62*, 294–310. [CrossRef]
41. Tahaei Yaghoubi, S.; Balobanov, V.; Mousavi, S.M.; Niiranen, J. Variational Formulations and Isogeometric Analysis for the Dynamics of Anisotropic Gradient-Elastic Euler-Bernoulli and Shear-Deformable Beams. *Eur. J. Mech.-A/Solids* **2018**, *69*, 113–123. [CrossRef]
42. Da Veiga, L.B.; Buffa, A.; Sangalli, G.; Vázquez, R. Mathematical Analysis of Variational Isogeometric Methods. *Acta Numer.* **2014**, *23*, 157–287.
43. Vázquez, R. A New Design for the Implementation of Isogeometric Analysis in Octave and Matlab: GeoPDEs 3.0. *Comput. Math. Appl.* **2016**, *72*, 523–554. [CrossRef]